AIChE

# Convection, Diffusion, and Exothermic Zero-Order Reaction in a Porous Catalyst Slab: Scaling and Perturbation Analysis

**João P. Lopes**
Laboratory of Separation and Reaction Engineering, Associate Laboratory LSRE/LCM, Dept. of Chemical Engineering, Faculty of Engineering, University of Porto, 4200-465 Porto, Portugal

**Silvana S. S. Cardoso**
Dept. of Chemical Engineering and Biotechnology, University of Cambridge, Cambridge CB2 3RA, U.K.

**Alírio E. Rodrigues**
Laboratory of Separation and Reaction Engineering, Associate Laboratory LSRE/LCM, Dept. of Chemical Engineering, Faculty of Engineering, University of Porto, 4200-465 Porto, Portugal

*DOI 10.1002/aic.11830*
*Published online July 17, 2009 in Wiley InterScience (www.interscience.wiley.com).*

*The analysis of the interaction between transport phenomena and chemical reaction inside large-pore catalyst particles needs to include intraparticular convection as an additional mass/heat transfer mechanism. In this work, we describe by a 3D regime diagram the global behavior of a permeable catalyst slab, where an exothermic, zero-order reaction is occurring. An order of magnitude estimate for the maximum temperature change is obtained by scaling techniques in each regime of operation. Specific operating regimes of fast mass/heat transport, dominant reaction and strong intraparticular convection, are then studied in more detail using perturbation analysis. The results include approximate concentration and temperature profiles, which allow the estimation of both the effectiveness factor and maximum temperature attained inside the catalyst in these regimes.* © 2009 American Institute of Chemical Engineers *AIChE J,* 55: 2686–2699, 2009

*Keywords: mathematical modeling, intraparticular convection, effectiveness factor, maximum temperature, perfusive particles*

## Introduction

"Large-pore" materials have been used in several reaction and separation engineering applications, namely as catalyst supports, HPLC packings, ceramic membranes, or supports for mammalian cell culture and biomass growth. The interest in using these permeable materials arises from the nonnegligible convective contribution to the total transport rate inside the particle when subjected to a pressure difference, as first recognized by Wheeler.[1] The presence of convective flow within the pores of a coarse-grained pellet was found to reduce internal mass transfer resistance, only when kinetics just becomes diffusion controlled.[2] The enhancement observed in a catalyst particle was quantified analytically for isothermal first[2] and zero-order reactions (slab[3] and spherical[4] geometries). These two simple reaction rates constitute the two well-known limits for the Michaelis-Menten equation, used to describe consumption of substrates in biological media.

Large-pore materials provide indeed easy access for cell attachment and growth, but cell culture scaffolds are

Correspondence concerning this article should be addressed to S. S. S. Cardoso at sssc1@cam.ac.uk

severely limited by diffusional resistance, which coupled with low diffusivity and solubility in liquid-phase, make nutrients (such as oxygen) poorly available. The importance of convective flux through carriers with large pores has been noticed for antibody production,[5] cell seeding in perfusive bioreactors[6–11] and plant root cultures for production of pharmaceuticals and flavors.[12] The zero-order reaction kinetics is frequently used to model oxygen uptake rate, because the Michaelis-Menten constant can be much lower than the bulk concentration value (Fassnacht and Pörtner[5] and Prince et al.[12]).

Most of the modeling work hitherto has been focused exclusively on isothermal conditions. However, many (bio)-chemical reactions are strongly heat generating, and the common assumption of negligible internal temperature gradients has to be carefully evaluated. In what concerns the problem of intraparticular convection, diffusion, and reaction under nonisothermal conditions, most studies at particle level have been numerical.[13,14] Cardoso and Rodrigues[15] presented a perturbation analysis for nonisothermal first-order reaction in a permeable catalyst slab. This work intends to extend the approximate analytical analysis to zero-order reactions. The purposes of this approach are as follows: (1) to define operating regimes and understand the transitions between them; (2) to provide the approximate effectiveness factor for each regime; and (3) to estimate the maximum temperature attained inside the catalyst. An improved understanding of convective enhancement on the performance of porous particles as catalysts/supports, coupled with nonisothermal effects, is extremely relevant for reactor design and carrier structure optimization.

## Operating regimes

### *Governing equations and model parameters*

We adopt a one-dimensional steady-state model for mass and energy transport in a permeable catalyst slab, undergoing an exothermic zero-order reaction, in an uniform flow field (with a priori specified superficial fluid velocity, $u$). The conservation equations are as follows:

$$\frac{dc}{dx} = \frac{1}{Pe_m}\frac{d^2c}{dx^2} - \frac{\phi^2}{Pe_m} r(T) \tag{1}$$

$$\frac{dT}{dx} = \frac{1}{Pe_h}\frac{d^2T}{dx^2} + \frac{\phi^2}{Pe_m}\,\beta\frac{Pe_m}{Pe_h}\frac{\hat{T}_s}{\Delta\hat{T}} r(T) \tag{2}$$

subject to

$$c(x = \pm 1) = 0 \tag{3}$$

and

$$T(x = \pm 1) = 0 \tag{4}$$

where the concentration of reactant ($\hat{c}$), temperature ($\hat{T}$), and transverse position within the slab ($\hat{x}$) were nondimensionalized as follows[16]:

$$x = \frac{\hat{x}}{L};\quad c = \frac{\hat{c} - \hat{c}_s}{\hat{c}_s};\ \text{and}\ T = \frac{\hat{T} - \hat{T}_s}{\Delta\hat{T}}. \tag{5}$$

The characteristic length scale is the slab half-thickness ($L$) and the correct scale for temperature deviation from its surface value, $\Delta\hat{T}$, is so far unknown. The dimensionless groups in Eqs. 1 and 2 are the Thiele modulus $\left(\phi^2 = L^2 k_s/(\hat{c}_s D)\right)$, Prater's parameter $\left(\beta = (-\Delta H) D\,\hat{c}_s/\left(\rho\, C_p\, \kappa\, \hat{T}_s\right)\right)$, and the intraparticular mass and heat Peclet numbers ($Pe_m = uL/D$ and $Pe_h = uL/\kappa$). The intrinsic kinetic constant at surface conditions and the heat of the exothermic reaction are denoted, respectively, by $k_s$ and $(-\Delta H)$. The properties for the fluid and solid phases are taken to be uniform. Therefore, the effective reactant mass diffusivity $D$ (which takes into account particle porosity and tortuosity) and the fluid-filled catalyst effective thermal diffusivity $\kappa\left(=\lambda/\rho\, C_p\right)$, and hence the Lewis' number $(Le = \kappa/D)$, are fixed for a given system. Also, the density of the catalyst matrix filled with fluid ($\rho$) and its specific heat ($C_p$) are constant. Surface conditions are denoted by the subscript $s$.

The reaction term $r(T)$ in Eqs. 1 and 2 is only operative if reactant exists:

$$r(T) = \begin{cases} \exp\left[\frac{\varphi T}{1+\eta T}\right], & c > -1 \\ 0, & c = -1 \end{cases} \tag{6}$$

where $\eta = \Delta\hat{T}/\hat{T}_s$ and $\varphi = \gamma\,\eta$ are at most of $O(1)$. The Arrhenius parameter, $\gamma = E_{act}/\left(R\,\hat{T}_s\right)$, is related to the reaction activation energy $E_{act}$ and is referred to the surface temperature value $\hat{T}_s$.

*Effectiveness Factor.* A measure for the overall performance of the catalyst slab is given by the effectiveness factor, which compares the average reaction rate with the one observed if reactant concentration and temperature in the whole particle equal surface conditions. We seek to understand the enhancement brought to this quantity which can be defined as

$$\text{Eff} = \frac{1}{2\phi^2}\left(\left.\frac{dc}{dx}\right|_{x=1} - \left.\frac{dc}{dx}\right|_{x=-1}\right). \tag{7}$$

### *Scaling and regime diagram*

We want to describe the behavior of the catalyst slab in regimes where two important processes balance at a global scale, that is, $x \sim O(1)$. Examining Eq. 1 with $r(T) \sim O(1)$, the following possibilities arise:

(a) Dominant convection and diffusion for $Pe_m \sim 1$ and $\phi^2/Pe_m << 1$,

(b) Dominant diffusion and reaction for $Pe_m << 1$ and $\phi^2 \sim 1$, and

(c) Dominant convection and reaction for $Pe_m >> 1$ and $\phi^2/Pe_m \sim 1$.

Also, limiting regimes in which only one mechanism dominates are conceivable. Because the only two parameters at play are $Pe_m$ and $\phi^2$, this information concerning mass conservation can be represented in a $\phi^2 - Pe_m$ plot.

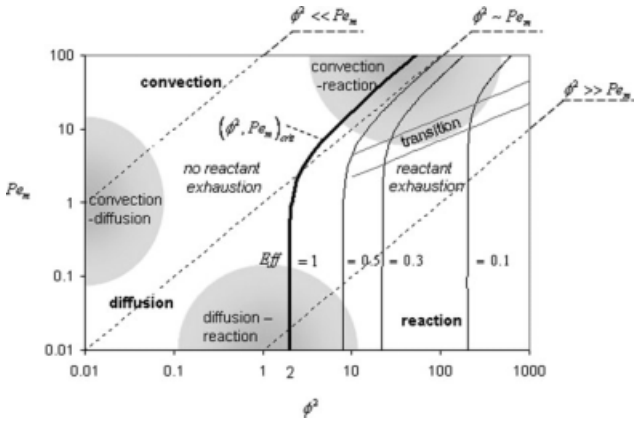


**Figure 1. Regime diagram for convection, diffusion and zero-order reaction in an isothermal catalyst slab (analytical results from Rodrigues et al.[3]).**

The boundary shown as a thick black line separates the situations of no reactant exhaustion (where Eff = 1) from the annulment region (where some iso-effectiveness factor curves at Eff<1 are represented).

*Isothermal Zero-Order Reaction in a Permeable Catalyst Slab.* For an isothermal system, exact analytical solutions are available.[3] The calculation of the effectiveness factor and the condition that separates the situation of reactant exhaustion from the one where no concentration annulment occurs, are of particular interest. These important results are represented in Figure 1. For representation convenience, we choose a factor of $10^{-2}$ to express smallness in the above magnitude relations. The regions where the system behaves globally as purely diffusive, convective, or reactive are shown, and the regimes described by a dominant balance between any of these two (gray areas). The thick-black line separates the parametric sets that lead to concentration annulment anywhere inside the particle from the situations where no reactant exhaustion occurs. This line of $\left(\phi^2, Pe_{\mathrm{m}}\right)_{\mathrm{crit}}$ is also the iso-effectiveness factor curve for Eff = 1, when reactant concentration reaches zero only at a single point inside the slab. We note that when concentration annulment occurs over a finite region, then the effectiveness factor is smaller than one. For $\left(\phi^2, Pe_{\mathrm{m}}\right) < \left(\phi^2, Pe_{\mathrm{m}}\right)_{\mathrm{crit}}$, no annulment occurs and Eff = 1. Outside this region, catalyst performance decreases with increasing Thiele modulus, as shown by the curves of constant effectiveness factor in the $\left(\phi^2, Pe_{\mathrm{m}}\right)$ plane. When $Pe_{\mathrm{m}} \to 0$, this boundary tends to the well-known diffusive limit of $\left(\phi^2\right)_{\mathrm{crit}} = 2$, and for $\phi^2 > 2$, the iso-effectiveness factor curves approach the value $\mathrm{Eff} = \sqrt{2}/\phi$ when $Pe_{\mathrm{m}} \to 0$. The effect of convection is visible for high $Pe_{\mathrm{m}}$, increasing the effectiveness factor for a given $\phi^2$ (and also the value of $\left(\phi^2\right)_{\mathrm{crit}}$ needed to achieve annulment), that is, the overall content of reactant inside the slab increases. The region around the gray lines represent the transition zone, above which, the effect of increasing the Peclet number (and therefore, convection) is particularly noticeable (this approximate criterion on will be derived later).

*Scaling for Temperature Change in Exothermic Systems.* To study nonisothermal systems, in which $\beta$ and $\gamma$ are fixed, we have to consider the intraparticular heat Peclet number, $Pe_{\mathrm{h}}$ (through the Lewis number, for example), in addition to $\phi^2$ and $Pe_{\mathrm{m}}$. A 3D regime diagram can be constructed by adding this third axis ($Le = Pe_{\mathrm{m}}/Pe_{\mathrm{h}}$), as shown in Figure 2.

An order of magnitude estimation and scaling for the characteristic temperature change, $\Delta\hat{T}$, can be obtained by a balance between the terms corresponding to the dominant effects in the energy balance.[17] To compare the magnitude between all terms in Eq. 2, we introduce a generic small parameter $\varepsilon$, which will express the relations between the dimensionless groups. Therefore, $\Delta\hat{T}/\Delta\hat{T}_{\mathrm{ad}} \sim \varepsilon\phi^2/Pe_{\mathrm{m}}$, $\varepsilon^{-1}\left(\phi^2/Pe_{\mathrm{m}}\right)$, or $\phi^2/Pe_{\mathrm{m}}$, when $Pe_{\mathrm{h}} \sim \varepsilon$, 1, or $\varepsilon^{-1}$, respectively (we shall take $>> \phi^2/Pe_{\mathrm{m}}$ as being $\sim \varepsilon^{-1}\left(\phi^2/Pe_{\mathrm{m}}\right)$).

In Figure 2, the results of temperature scaling in the planes of small and high $Pe_{\mathrm{m}}$ or $\phi^2$ are shown, and, for $Le \sim \varepsilon$. Because for a given system, the Lewis number is approximately constant, we show in detail the planes for $Le$ of order 1, $\varepsilon$, and $\varepsilon^{-1}$ (Figure 3). The boundaries between each region are schematic.

The indicated characteristic temperature changes are observed at an $O(1)$ scale inside the catalyst, and they account for the existence of reaction throughout the slab.

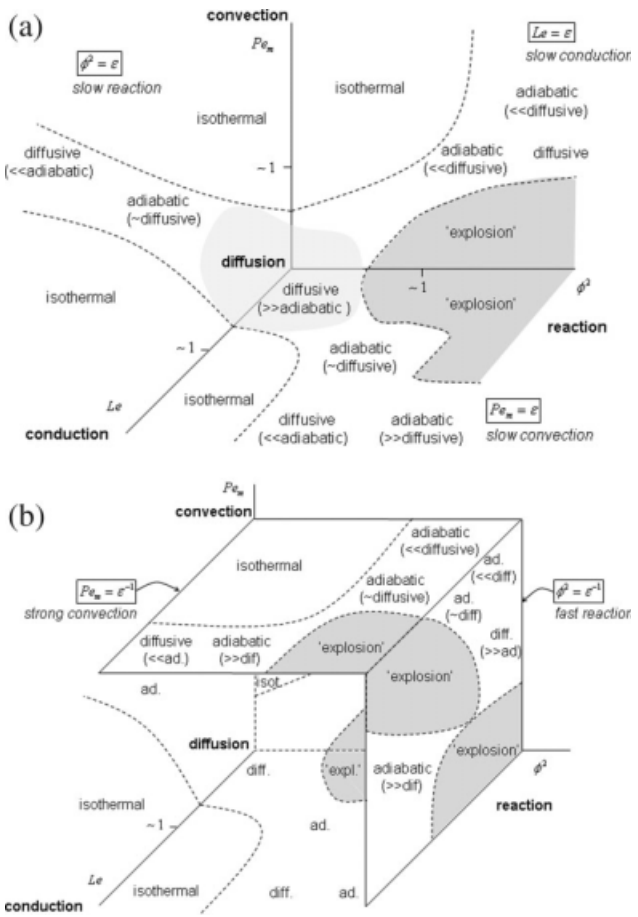


**Figure 2. 3D regime diagram for convection, diffusion, and exothermic reaction in a catalyst slab.**

The regions marked as isothermal present very small deviation from surface temperature. The adiabatic (ad.) limit is related to the characteristic temperature change under diffusive conditions (diff., $\Delta\hat{T}_{\mathrm{dif}} = \beta\hat{T}_{\mathrm{s}}$) by the Lewis number: $\Delta\hat{T}_{\mathrm{ad}} = \Delta\hat{T}_{\mathrm{dif}}\,Le$. When $\Delta\hat{T} >> \Delta\hat{T}_{\mathrm{ad}}, \Delta\hat{T}_{\mathrm{dif}}$, "explosion" (expl.) occurs. (a) $Le = \varepsilon, Pe_{\mathrm{m}} = \varepsilon$, and $\phi^2 = \varepsilon$ planes. (b) $Pe_{\mathrm{m}} = \varepsilon^{-1}$ and $\phi^2 = \varepsilon^{-1}$ planes.

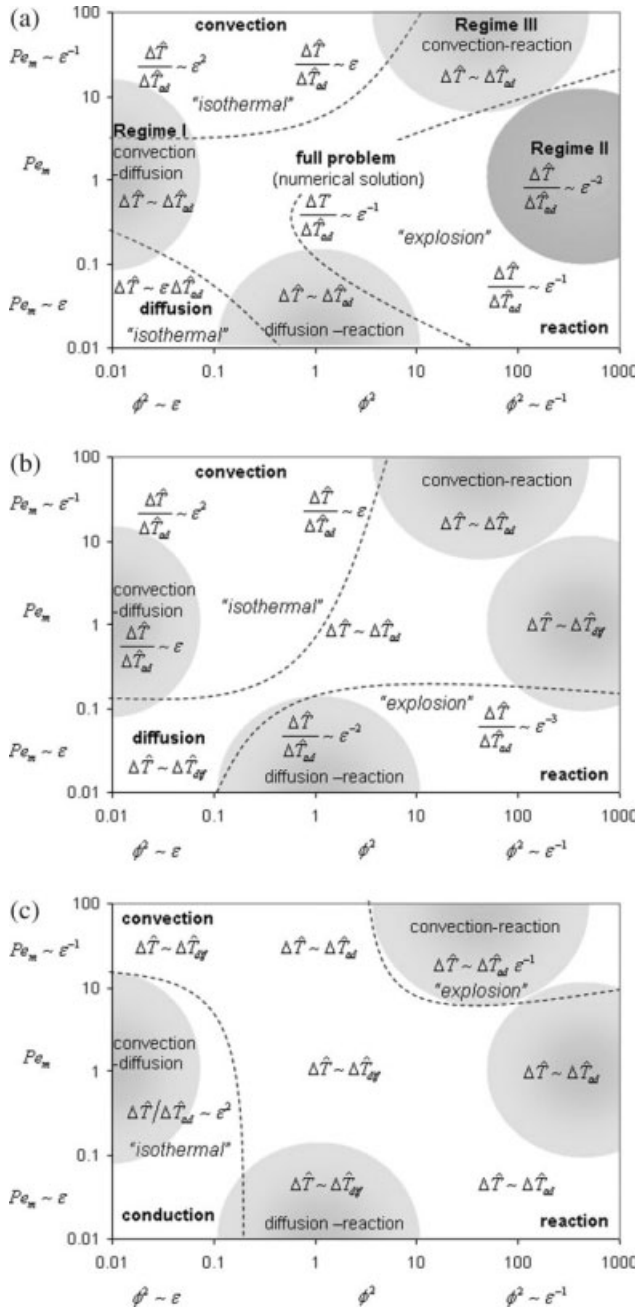


**Figure 3. Regime diagram for exothermic reaction inside permeable porous catalyst slab (planes for $Le$ of order 1, $\varepsilon$, and $\varepsilon^{-1}$).**

(a) $Le \sim 1$ ($\Delta\hat{T}_{ad} \sim \Delta\hat{T}_{dif}$); (b) $Le \sim \varepsilon$ ($\Delta\hat{T}_{ad} \sim \varepsilon\,\Delta\hat{T}_{dif}$); and (c) $Le \sim \varepsilon^{-1}$ ($\Delta T_{dif} \sim \varepsilon\,\Delta T_{ad}$).

However, the existence of a reactant limitation (which puts an end to the heat-generating reaction) stops the increase of temperature. To obtain a correct estimate for temperature change, "active" regions of thickness much smaller than 1 have to be considered (because the solution already includes an $O(1)$ branch from Eqs. 1 to 2 with $r(T) = 0$). For example, in the identified "explosive" regions, the maximum temperature predicted in each one of the $Le =$ constant planes decreases from $\Delta\hat{T} \sim \Delta\hat{T}_{ad}\,\varepsilon^{-1}$ to $\Delta\hat{T}_{ad}$ and then to $\Delta\hat{T}_{ad}\,\varepsilon$, when Lewis number increases ($Le \sim \varepsilon,\ 1,\ \varepsilon^{-1}$). This can be explained by the increasingly stronger heat loss by conduction to the cold boundaries, when compared with species diffusion rate to the reactive zones.

Because the rest of this work focuses on the particular case of $Le \sim 1$ (Figure 3a), we take $\Delta\hat{T}_{ad}$ as a scale for temperature change in the regimes of slow and fast reaction (Regime I and II, respectively) and strong intraparticular convection (Regime III). With this scale, Eqs. 1 and 2 become:

$$\frac{dc}{dx} = \frac{1}{Pe_m}\frac{d^2c}{dx^2} - \frac{\phi^2}{Pe_m}r(T) \tag{8}$$

$$\frac{dT}{dx} = \frac{1}{Pe_m}\frac{Pe_m}{Pe_h}\frac{d^2T}{dx^2} + \frac{\phi^2}{Pe_m}\,r(T) \tag{9}$$

The reaction term was assumed of $O(1)$

$$r(T) = \exp\left[\frac{\varphi T}{1+\eta T}\right] = \exp\left[\frac{\gamma\,\beta\,Le\,T}{1+\beta\,Le\,T}\right] \sim \exp[\gamma\,\beta\,Le\,T]$$

for $Le$ and $T \sim O(1)$. The product $\gamma\beta$ can also be taken close to unity for common exothermic reactions,[18] because $\beta$ rarely exceeds 0.3 and the typical range for $\gamma$ is $\sim 10 - 30$.

### *Perturbation analysis*

The limiting cases discussed in the previous section can be analyzed in more depth by considering appropriate parameter regimes and conducting a perturbation analysis.[19] The results in the present work apply to $Le \sim O(1)$ and they intend to approximate the full solution of the complete problem in the limits of: fast mass/heat transport (Regime I), dominant reaction (Regime II), and strong intraparticular convection (Regime III). The diffusive regime for an exothermic zero-order reaction (diffusion-reaction gray area in Figure 3 and $Pe_m = 0$ plane in Figure 2a) was studied, among others, by Frank-Kamenetskii,[20] Hlavacek and Marek[21] and Aris,[22] and will be used to validate our solutions.

### *Regime I (Chemical regime)*

When transport mechanisms are much faster than chemical reaction, concentration and temperature inside the slab depart little from its surface values (Figure 4). This corresponds to the case when Thiele modulus is low and to the classic chemical regime, in the presence of convection.

We take $\varepsilon = \phi^2/Pe_m$ as perturbation parameter and look for regular perturbation solutions of Eqs. 8 and 9, under the following conditions:

$$\frac{\phi^2}{Pe_m} << 1, \frac{1}{Pe_m}, \frac{1}{Pe_h} \tag{10}$$

Also, in this regime, concentration annulment is not expected to occur, so the appropriate form of Eqs. 8 and 9 takes into account the reaction term. The uniformly valid solutions are assumed to be of the following form:

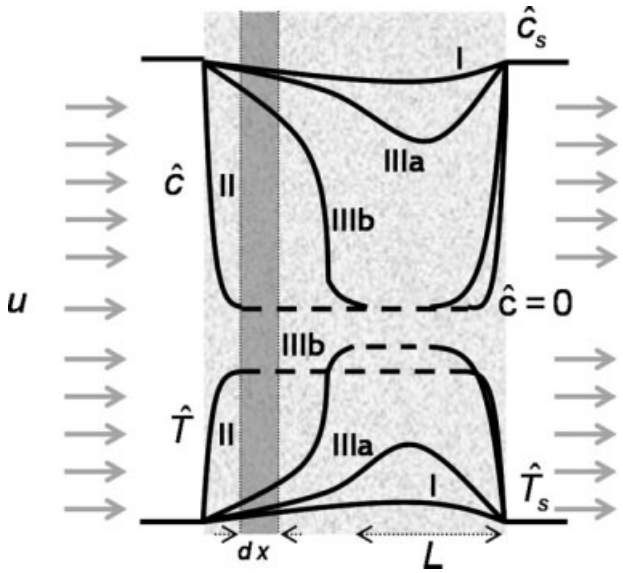


**Figure 4. Schematic concentration and temperature profiles in a permeable catalyst slab, where an exothermic zero-order reaction occurs.**

The regimes studied are slow and fast reaction (Regime I and II, respectively) and strong convection with and without (Regime IIIb and Regime IIIa, respectively) concentration annulment.

$$c(x;\ \varepsilon) = \sum_{n=0}^{\infty} c_{\mathrm{n}}(x)\ \varepsilon^n \tag{11}$$

and

$$T(x;\ \varepsilon) = \sum_{n=0}^{\infty} T_{\mathrm{n}}(x)\ \varepsilon^n \tag{12}$$

The effect of reaction is felt at $O\left(\phi^2/Pe_{\mathrm{m}}\right)$, but because it is calculated from surface conditions (zero-order solution, $c_0(x) = 0$ and $T_0(x) = 0$), the order of the reaction is, so far, irrelevant. Therefore, the solutions up to $O(\varepsilon)$ equal the ones obtained by perturbation techniques[15] for first-order reaction:

$$c(x) = \frac{\phi^2}{Pe_{\mathrm{m}}}\left[\frac{2\,e^{Pe_{\mathrm{m}}\,(x+1)}}{e^{2Pe_{\mathrm{m}}}-1} - \frac{e^{2Pe_{\mathrm{m}}}+1}{e^{2Pe_{\mathrm{m}}}-1} - x\right] + O\left(\frac{\phi^4}{Pe_{\mathrm{m}}^2}\right) \tag{13}$$

$$T(x) = \frac{\phi^2}{Pe_{\mathrm{m}}}\left[\frac{2\,e^{Pe_{\mathrm{h}}\,(x+1)}}{1-e^{2Pe_{\mathrm{h}}}} + \frac{e^{2Pe_{\mathrm{h}}}+1}{e^{2Pe_{\mathrm{h}}}-1} + x\right] + O\left(\frac{\phi^4}{Pe_{\mathrm{m}}^2}\right). \tag{14}$$

Equation 13 reproduce the solution for the problem of convection, diffusion, and isothermal zero-order reaction in a slab,[3] as no information regarding the nonisothermal behavior of the system is included. Nevertheless, the two-term expansion is enough to represent concentration and temperature profiles accurately.

Concentration and temperature profiles (Eqs. 13 and 14) are represented in Figure 5. Numerical results obtained with gPROMS[23] are also plotted. The agreement is especially good for $\varepsilon \sim 0.01$.

For an exothermic reaction, the maximum temperature occurs at:

$$x_{\max} = -1 + \frac{1}{Pe_{\mathrm{h}}}\ln\left[\frac{e^{2Pe_{\mathrm{h}}}-1}{2Pe_{\mathrm{h}}}\right] \tag{15}$$

whereas the minimum concentration occurs at

$$x_{\min} = -1 + \frac{1}{Pe_{\mathrm{m}}}\ln\left[\frac{e^{2Pe_{\mathrm{m}}}-1}{2Pe_{\mathrm{m}}}\right]. \tag{16}$$

$x_{\min}$ and $x_{\max}$ are, in general, distinct (as long as $Le \neq 1$). The minimum concentration value in this regime is of order $\varepsilon$, and is given by:

$$c^{\min} = -\frac{\phi^2}{Pe_{\mathrm{m}}}\left[\frac{2}{e^{2Pe_{\mathrm{m}}}-1} - \frac{1}{Pe_{\mathrm{m}}} + \frac{1}{Pe_{\mathrm{m}}}\ln\left(\frac{e^{2Pe_{\mathrm{m}}}-1}{2Pe_{\mathrm{m}}}\right)\right]. \tag{17}$$

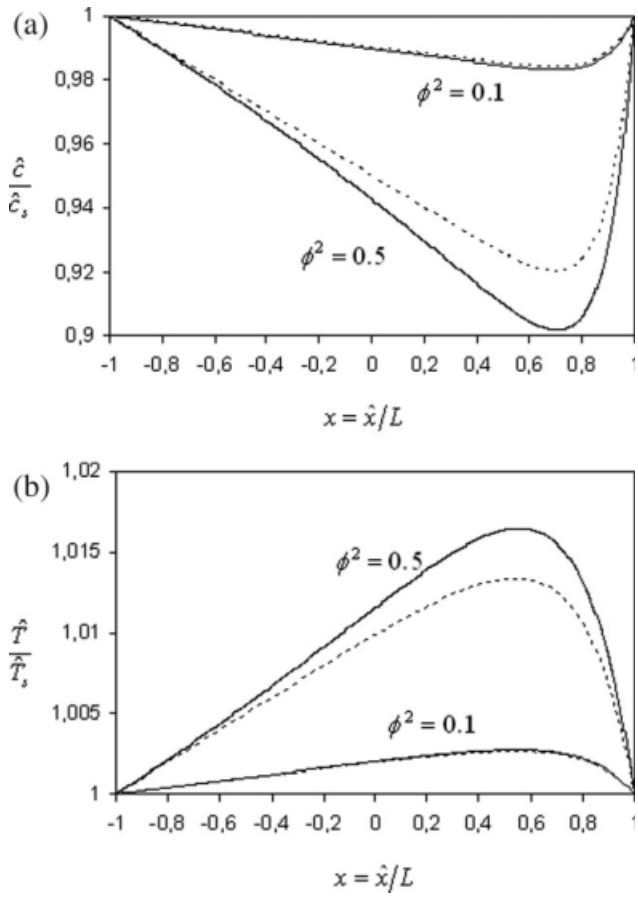


**Figure 5. Comparison of the perturbation solutions (Eqs. 13 and 14, dashed lines) with numerical results from gPROMS[23] (solid lines) for $\gamma$ = 20, $\beta$ = 0.1, $Pe_{\mathrm{m}}$ = 10, $Pe_{\mathrm{h}}$ = 5, and $\phi^2$ = 0.1 ($\varepsilon$ = 0.01) or $\phi^2$ = 0.5 ($\varepsilon$ = 0.05).**

(a) Reactant concentration profile. (b) Temperature profile.

Because thermal effects do not affect the concentration profile for weak reaction conditions, Eqs. 16 and 17 reproduce the isothermal results,[3] when no annulment occurs. An estimate for maximum temperature will be given later.

***Regime II (Diffusional regime)***

The regime in which reaction is fast compared with transport mechanisms appears for large Thiele modulus. To study this diffusional regime (in the presence of convection), we set the perturbation parameter to $\varepsilon = Pe_m/\phi^2$. Under the conditions:

$$\frac{\phi^2}{Pe_m} >> 1, \frac{1}{Pe_m}, \frac{1}{Pe_h} \tag{18}$$

the solution to Eqs. 8 and 9 is obtained by conducting a singular perturbation analysis. We expect boundary layers to occur near the slab surfaces, where reactant concentration decreases and temperature increases sharply from the middle solution to surface values (Figure 4).

*Middle Region*. The outer reduced problem from Eqs. 8 to 9 with the chemical reaction term has no physical solution. Consequently, chemistry-free equations should be used in this region. They are written as:

$$c^m(x) = -1 \quad \text{for } x' \le x \le x^*, \tag{19}$$

$$\frac{dT^m}{dx} = \frac{1}{Pe_h}\frac{d^2T^m}{dx^2} \quad \text{for } x' \le x \le x^*. \tag{20}$$

The solution of Eq. 20 is intended to represent the temperature profile in the region where reactant disappears (between $x'$ and $x^*$). Additionally, boundary layer regions at $x = \pm 1$ bring surface temperature to match the middle region profile. Also, continuity in profile and in the flux (i.e., null derivative) is required at $x'$ or $x^*$ (where the maximum temperature occurs). Therefore, a reasonable simplification for the middle section temperature is a plateau at its maximum value:

$$T^m(x;\varepsilon) = T^{\max}(\varepsilon) = T_0^{\max} + T_1^{\max}\sqrt{\varepsilon} + O(\varepsilon). \tag{21}$$

*Right Boundary Layer*. At the inner layer near $x = 1$, the reaction-diffusion distinguished limit suggests the following stretching transformation:

$$X = \frac{1-x}{\sqrt{\varepsilon}}. \tag{22}$$

Equations 8 and 9 then become:

$$\frac{1}{Pe_m}\frac{d^2c^r}{dX^2} + \sqrt{\varepsilon}\frac{dc^r}{dX} - \exp\left[\frac{\varphi T^r}{1+\eta T^r}\right] = 0 \quad \text{for } 0 \le X \le X^* \tag{23}$$

$$\frac{1}{Pe_h}\frac{d^2T^r}{dX^2} + \sqrt{\varepsilon}\frac{dT^r}{dX} + \exp\left[\frac{\varphi T^r}{1+\eta T^r}\right] = 0 \quad \text{for } 0 \le X \le X^* \tag{24}$$

subject to boundary,

$$c^r(X=0) = 0 \tag{25}$$

and

$$T^r(X=0) = 0 \tag{26}$$

profile continuity,

$$c_n^r(X^*) = c_n^m(x^*) = \begin{cases} -1, & n = 0 \\ 0, & n \ge 1 \end{cases} \tag{27}$$

$$T_n^r(X^*) = T_n^m(x^*) = T_n^{\max} \tag{28}$$

and derivative continuity conditions,

$$\lim_{\varepsilon\to 0} \left.\frac{dc^r}{dX}\right|_{X^*,\varepsilon} = 0 \tag{29}$$

$$\lim_{\varepsilon\to 0} \frac{1}{\sqrt{\varepsilon}}\left[\left.\frac{dc^r}{dX}\right|_{X^*,\varepsilon} - \left.\frac{dc^r}{dX}\right|_{X^*,\varepsilon=0}\right] = 0 \tag{30}$$

(similar equations similar to 29 and 30 should be written for temperature profile, $T^r(X)$).

*Left Boundary Layer*. At the slab's "entrance," the proper rescaling is given by:

$$Y = \frac{1+x}{\sqrt{\varepsilon}} \tag{31}$$

predicted from the diffusive-reactive nature of the boundary layer (same reasoning as for the boundary layer on the right). The equations for this region are as follows:

$$\frac{1}{Pe_m}\frac{d^2c^l}{dY^2} - \sqrt{\varepsilon}\frac{dc^l}{dY} - \exp\left[\frac{\varphi T^l}{1+\eta T^l}\right] = 0 \quad \text{for } 0 \le Y \le Y' \tag{32}$$

$$\frac{1}{Pe_h}\frac{d^2T^l}{dY^2} - \sqrt{\varepsilon}\frac{dT^l}{dY} + \exp\left[\frac{\varphi T^l}{1+\eta T^l}\right] = 0 \quad \text{for } 0 \le Y \le Y' \tag{33}$$

subject to:

$$c^l(Y=0) = 0 \tag{34}$$

and

$$T^l(Y=0) = 0 \tag{35}$$

$$c_n^l(Y') = c_n^m(x') = \begin{cases} -1, & n = 0 \\ 0, & n \ge 1 \end{cases} \tag{36}$$

$$T_{\mathrm{n}}^{l}(Y') = T_{\mathrm{n}}^{m}(x') = T_{\mathrm{n}}^{\max} \tag{37}$$

$$\lim_{\varepsilon\to 0} \left.\frac{dc^{l}}{dY}\right|_{Y',\varepsilon} = 0 \tag{38}$$

$$\lim_{\varepsilon\to 0} \frac{1}{\sqrt{\varepsilon}} \left[\left.\frac{dc^{l}}{dY}\right|_{Y',\varepsilon} - \left.\frac{dc^{l}}{dY}\right|_{Y',\varepsilon=0}\right] = 0 \tag{39}$$

(similar conditions for temperature profile $T^{l}(Y)$ are written in analogy with Eqs. 38 and 39).

*Approximate Concentration and Temperature Profiles.* After solving the set of Eqs. 23–30 and 32–39, it is possible to describe the concentration and temperature profiles by branches:

$$c(x;\,\varepsilon) = \begin{cases} \sum_{n=0}^{\infty} c_{\mathrm{n}}^{l}(x)\;\varepsilon^{n/2}, & -1 \le x \le x' \\ -1, & x' \le x \le x^{*} \\ \sum_{n=0}^{\infty} c_{\mathrm{n}}^{r}(x)\;\varepsilon^{n/2}, & x^{*} \le x \le 1 \end{cases} \tag{40}$$

$$T(x;\,\varepsilon) = \begin{cases} \sum_{n=0}^{\infty} T_{\mathrm{n}}^{l}(x)\;\varepsilon^{n/2}, & -1 \le x \le x' \\ T^{\max}(\varepsilon), & x' \le x \le x^{*} \\ \sum_{n=0}^{\infty} T_{\mathrm{n}}^{r}(x)\;\varepsilon^{n/2}, & x^{*} \le x \le 1 \end{cases} \tag{41}$$

with $X^{*} = (1-x^{*})/\sqrt{\varepsilon} = \sum_{n=0}^{\infty} X_{\mathrm{n}}^{*}\;\varepsilon^{n/2}$ and $Y' = (-1+x')/\sqrt{\varepsilon} = \sum_{n=0}^{\infty} Y_{\mathrm{n}}^{'}\;\varepsilon^{n/2}$.

After expressing the nonlinear term in Eq. 6 by a Taylor series around $\varepsilon = 0$, and making the following approximations:

$$\exp\left[\frac{\varphi T_0^{r}}{1+\eta T_0^{r}}\right] \sim b^{2} \tag{42}$$

$$\frac{\varphi\, T_1^{r}}{\left(1+\eta T_0^{r}\right)^{2}} \exp\left[\frac{\varphi T_0^{r}}{1+\eta T_0^{r}}\right] \sim d \tag{43}$$

and

$$\frac{\varphi\, T_1^{l}}{\left(1+\eta T_0^{l}\right)^{2}} \exp\left[\frac{\varphi T_0^{l}}{1+\eta T_0^{l}}\right] \sim f \tag{44}$$

it is possible to find simple analytical solutions to the subproblems arising from Eqs. 23, 24, 32 and 33. At leading order, these solutions are as follows:

$$c_0^{r}(X) = -\frac{X}{X^{*}} + \frac{Pe_{\mathrm{m}}\, b^{2}}{2}(X - X^{*})X \tag{45}$$

$$T_0^{r}(X) = T_0^{\max}\frac{X}{X^{*}} - \frac{Pe_{\mathrm{h}}\, b^{2}}{2}(X - X^{*})X \tag{46}$$

$$c_0^{l}(Y) = -\frac{Y}{Y'} + \frac{Pe_{\mathrm{m}}\, b^{2}}{2}(Y - Y')Y \tag{47}$$

$$T_0^{l}(Y) = T_0^{\max}\frac{Y}{Y'} - \frac{Pe_{\mathrm{h}}\, b^{2}}{2}(Y - Y')Y \tag{48}$$

with

$$T_0^{\max} = \frac{Pe_{\mathrm{h}}}{Pe_{\mathrm{m}}}, \tag{49}$$

$$X_0^{*} = \sqrt{\frac{2}{Pe_{\mathrm{m}} b^{2}}}, \tag{50}$$

and

$$Y_0' = \sqrt{\frac{2}{Pe_{\mathrm{m}} b^{2}}}. \tag{51}$$

Finally, the concentration and temperature profile corrections at $O(\sqrt{\varepsilon})$ are as follows:

$$c_1^{r}(X) = \frac{Pe_{\mathrm{m}}}{2}\,X\,(X - X^{*})\left[X^{*} + d - \frac{b^{2} Pe_{\mathrm{m}}}{3}\left(X - \frac{X^{*}}{2}\right)\right] \tag{52}$$

$$T_1^{r}(X) = \frac{X}{X^{*}}\left\{T_1^{\max} - Pe_{\mathrm{h}}(X - X^{*}) \times \left[\frac{T_0^{\max}}{2} + \frac{d}{2}X^{*} + \frac{b^{2} Pe_{\mathrm{h}}}{6}X^{*}\left(-X + \frac{X^{*}}{2}\right)\right]\right\} \tag{53}$$

and

$$c_1^{l}(Y) = \frac{Pe_{\mathrm{m}}\,Y}{2}\,(Y - Y')\left[-\frac{1}{Y'} + f + \frac{b^{2} Pe_{\mathrm{m}}}{3}\left(Y - \frac{Y'}{2}\right)\right] \tag{54}$$

$$T_1^{l}(Y) = Y\left\{\frac{T_1^{\max}}{Y'} - Pe_{\mathrm{h}}(Y - Y') \times \left[-\frac{T_0^{\max}}{2Y'} + \frac{f}{2} + \frac{b^{2} Pe_{\mathrm{m}}}{6}\left(Y - \frac{Y'}{2}\right)\right]\right\}. \tag{55}$$

The convective corrections to the annulment positions are calculated from Eqs. 30 to 39:

$$X_1{}^{*} = -\frac{1}{b^{2}}\left(\frac{1}{3} + \frac{\sqrt{2}\,d}{2\,b\,\sqrt{Pe_{\mathrm{m}}}}\right), \tag{56}$$

$$Y_1' = \frac{1}{b^{2}}\left(\frac{1}{3} - \frac{\sqrt{2}f}{2\,b\,\sqrt{Pe_{\mathrm{m}}}}\right). \tag{57}$$

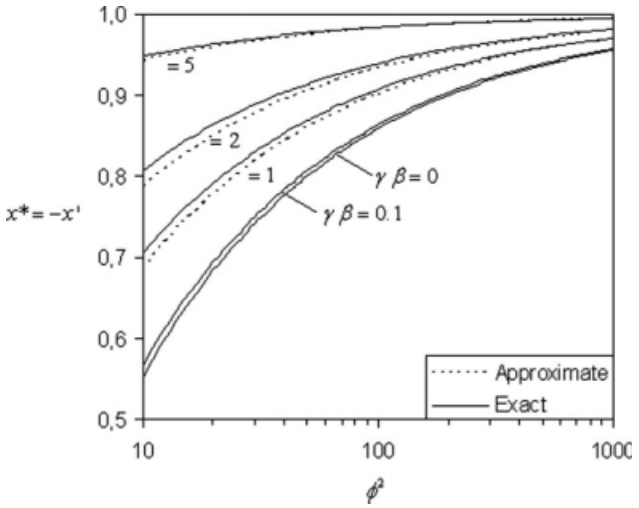


**Figure 6. Concentration annulment positions in the diffusive limit for an exothermic zero-order reaction.**

Comparison between the exact analytical solution[22] and perturbation solutions in the limit of negligible convection (Eqs. 50 and 51 with 61). For $\gamma\beta \leq 0.1$, exact and approximate results coincide.

When similar equations are written for temperature, two estimates for the maximum temperature correction arise. They can be expressed by $T_1^{\max} = \frac{\sqrt{2}Pe_h}{3b\sqrt{Pe_m}}\frac{Pe_h}{Pe_m}\left|1-\frac{Pe_m}{Pe_h}\right|$. The constants $\boldsymbol{b^2}$, $d$, and $f$ are determined by an integral method where the approximated solutions are required to satisfy simplified differential equations and boundary conditions on average over the thickness of the boundary layers (a similar approximation is described elsewhere[15,16]). So, for $\eta T << 1$, the conditions for these constants determination are as follows:

$$\int_0^{X_0^*}\left\{\frac{1}{Pe_h}\frac{d^2T_0^r}{dX^2}+\exp\left[\varphi T_0^r\right]\right\}dX=0, \tag{58}$$

$$\int_0^{X_0^*}\left\{\frac{1}{Pe_h}\frac{d^2T_1^r}{dX^2}+\varphi\, b^2\, T_1^r+\frac{dT_0^r}{dX}\right\}dX=0, \tag{59}$$

$$\int_0^{Y_0'}\left\{\frac{1}{Pe_h}\frac{d^2T_1^l}{dY^2}+\varphi\, b^2\, T_1^l-\frac{dT_0^l}{dY}\right\}dY=0. \tag{60}$$

Integrating Eqs. 58–60, after substitution of the previous approximate temperature profiles (Eqs. 46, 53, and 55), yields:

$$b^2=\frac{\sqrt{\pi}}{2}\exp\left(\varphi\frac{Pe_h}{Pe_m}\right)\frac{erf\sqrt{\varphi\,\frac{Pe_h}{Pe_m}}}{\sqrt{\varphi\,\frac{Pe_h}{Pe_m}}}, \tag{61}$$

$$d=\frac{\varphi\, b\, Pe_h}{\sqrt{2\,Pe_m}}\,\frac{1+2|1-Pe_m/Pe_h|}{6Pe_m/Pe_h-\varphi}, \tag{62}$$

and

$$f=-\frac{\varphi\, b\, Pe_h}{\sqrt{2\,Pe_m}}\,\frac{1-2|1-Pe_m/Pe_h|}{6Pe_m/Pe_h-\varphi}. \tag{63}$$

The leading-order problem in the boundary layers assumes a reaction-diffusion dominant balance, so the solution given by Eqs. 45–51 and 61 can be directly compared with the exact analytical solutions at high Thiele modulus for the problem of exothermic zero-order reaction in a catalyst slab where mass/heat transfer occurs solely by diffusion/conduction. For slab geometry, when $\gamma\beta\phi^2 > 0.878$ (at high Thiele modulus), there is only one steady state solution for the diffusive-reactive problem[20,22,24] with

$$x^* = (-x') = 1-\frac{\sqrt{2}}{\phi}\,\frac{\mathrm{sech}^{-1}e^{-\gamma\beta/2}}{\sqrt{\gamma\beta\, e^{\gamma\beta}}}. \tag{64}$$

This result agrees with our perturbation solutions, Eqs. 50 and 51, if $b \sim \sqrt{\gamma\beta\, e^{\gamma\beta}}\Big/\mathrm{sech}^{-1}\left(e^{-\gamma\beta/2}\right)$, with $b$ from Eq. 61. This comparison is plotted in Figure 6 for several values of $\gamma\beta$.

At high Thiele modulus, the temperature and concentration variation is concentrated in thin boundary layers, so the parabolic approximation in Eqs. 45–48 is a reasonable one, which proves to be in excellent agreement with exact analytical results,[22] as shown in Figure 7. The leading-order temperature profile in the middle region (Eq. 49) is Prater's maximum temperature estimate for reaction-diffusion problems.

In the isothermal limit ($\varphi \to 0$, $b^2 \to 1$, and $d,f \to 0$), $x^*$ and $x'$ calculated from Eqs. 50, 51, 56 and 57 yield

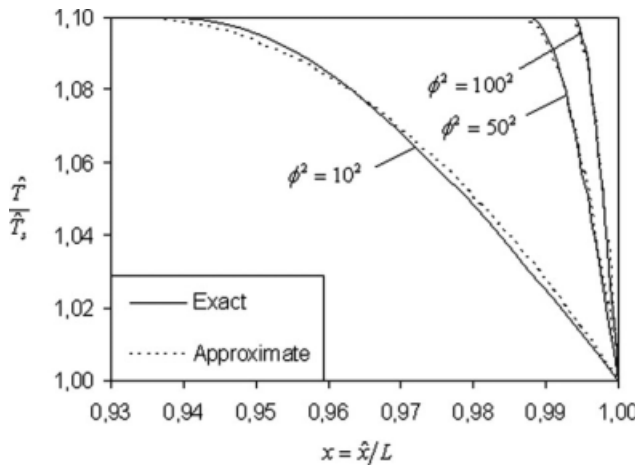


**Figure 7. Temperature profiles in the right boundary layer (next to $x = 1$) in the diffusional regime for $\gamma = 20$, $\beta = 0.1$, $Pe_m = 10$, $Pe_h = 5$, and $\phi = 10,50,100$.**

The leading-order perturbation solutions (dashed lines) are compared with the exact analytical results (solid lines) by Aris.[22]

$$x^* \to 1 - \sqrt{\frac{2}{Pe_m}}\sqrt{\varepsilon} + \frac{1}{3}\varepsilon + O\left(\varepsilon^{3/2}\right), \tag{65}$$

$$x' \to -1 + \sqrt{\frac{2}{Pe_m}}\sqrt{\varepsilon} + \frac{1}{3}\varepsilon + O\left(\varepsilon^{3/2}\right). \tag{66}$$

In the analysis of convection and diffusion with zero-order isothermal reaction, Rodrigues et al.[3] calculate $x^*$ and $x'$ by solving numerically two nonlinear algebraic equations. We can find an approximate solution for those equations by perturbation techniques, for $\varepsilon = Pe_m/\phi^2 << 1$. The result of that calculation reproduces Eqs. 65 and 66.

### *Regime III (Strong intraparticular convection regime)*

A third regime, where intraparticular convection dominates mass and heat transport, can be studied for parameters obeying the following conditions:

$$\frac{\phi^2}{Pe_m} \sim 1 \text{ and } \frac{1}{Pe_h}, \frac{1}{Pe_m} << 1. \tag{67}$$

Therefore, $\varepsilon = 1/Pe_m$ is taken as the perturbation parameter (also $1/Pe_h \sim \varepsilon$). Because the reaction term in Eq. 6 is defined by two branches, the situation with concentration annulment needs to be treated separately from the one where no reactant exhaustion occurs.

*No Annulment of Reactant Concentration Inside the Particle (Regime IIIa).* In this situation, the solution structure includes an outer region in the left-middle section of the slab and a boundary layer next to $x = 1$. For $\eta T_0^l << 1$, the leading order solution for most part of the slab is

$$T_0^l = -\frac{1}{\varphi}\ln\left[1 - \frac{\varphi\,\phi^2}{Pe_m}(x+1)\right] \tag{68}$$

and

$$c_0^l = -T_0^l = \frac{1}{\varphi}\ln\left[1 - \frac{\varphi\,\phi^2}{Pe_m}(x+1)\right]. \tag{69}$$

In the diffusive-convective boundary layer at the slab's right surface,

$$c_0^r(Y) = a_1\left[1 - \exp(-Y)\right] \tag{70}$$

$$T_0^r(Y) = a_2\left[1 - \exp\left(-\frac{Pe_h}{Pe_m}Y\right)\right] \tag{71}$$

where $Y = (1-x)/\varepsilon$ and the integration constants are $a_1$ and $a_2$ (determined by matching with the outer solution, Eqs. 68 and 69). With $O(1)$ terms, the matching principle is simply[19]:

$$\lim_{Y\to\infty} c_0^r = \lim_{x\to 1} c_0^l$$

$$\lim_{Y\to\infty} T_0^r = \lim_{x\to 1} T_0^l.$$

Taking the limits of Eqs. 68–71:

$$a_1 = -a_2 = \frac{1}{\varphi}\ln\left[1 - \frac{2\varphi\,\phi^2}{Pe_m}\right]. \tag{72}$$

Matching between the two solutions is possible only if

$$\frac{2\varphi\,\phi^2}{Pe_m} < 1. \tag{73}$$

If condition in Eq. 73 is not met then a solution valid for the whole slab can not be obtained. This suggests that, for typical parameter values, these solutions are only suitable for low Thiele modulus range. They will be useful for describing a regime near the "chemical regime," but with strong convection. An additional term was calculated at $O(\varepsilon)$, but it was found to have negligible contribution to the complete solution.

*Composite Solution.* The final composite solution, valid across the whole catalyst, is given by

$$c_0^{\text{comp}}(x) = c_0^l(x) + c_0^r(Pe_m(1-x)) - \lim_{Y\to\infty} c_0^r(Y), \tag{74}$$

$$T_0^{\text{comp}}(x) = T_0^l(x) + T_0^r(Pe_m(1-x)) - \lim_{Y\to\infty} T_0^r(Y). \tag{75}$$

Substituting Eqs. 68–71 into Eqs. 74–75:

$$c(x) = \frac{1}{\varphi}\ln\left[1 - \frac{\varphi\,\phi^2}{Pe_m}(x+1)\right] - \frac{1}{\varphi}\ln\left[1 - \frac{2\varphi\,\phi^2}{Pe_m}\right] e^{-Pe_m(1-x)} + O\left(\frac{1}{Pe_m}\right) \tag{76}$$

$$T(x) = -\frac{1}{\varphi}\ln\left[1 - \frac{\varphi\,\phi^2}{Pe_m}(x+1)\right] + \frac{1}{\varphi}\ln\left[1 - \frac{2\varphi\,\phi^2}{Pe_m}\right] e^{-Pe_h(1-x)} + O\left(\frac{1}{Pe_m}\right). \tag{77}$$

Figure 8 provides a comparison of the analytical results (Eqs. 76 and 77) with numerical solutions from gPROMS.[23] The outer and inner branches of the solution (Eqs. 68, 69, 70 and 71, respectively) are also represented.

In this regime, we expect the minimum concentration to be close to surface concentration. We calculate it from $dc/dx|_{x_{\min}} = 0$, which yields

$$c^{\min} = \frac{1}{\varphi}\ln\left[1 - \frac{\varphi\,\phi^2}{Pe_m}(x_{\min}+1)\right] - \frac{1}{\varphi}\ln\left[1 - \frac{2\varphi\,\phi^2}{Pe_m}\right] e^{-Pe_m(1-x_{\min})} \tag{78}$$

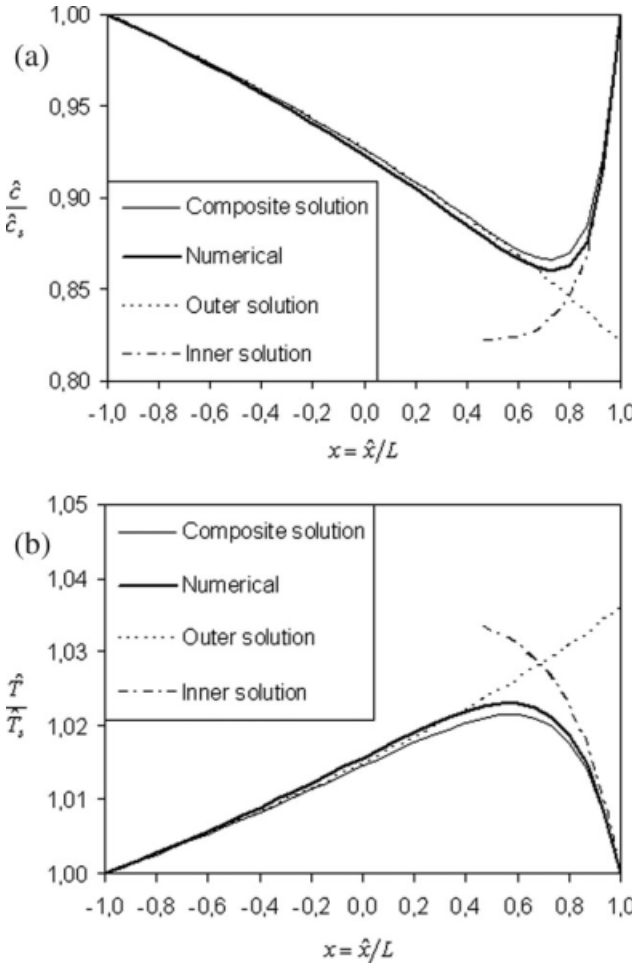


**Figure 8. Comparison between composite solutions Eqs. 76 and 77, numerical results and contributions from outer and inner regions for $\varphi = 4$, $\phi^2 = 0.8^2$, $Pe_m = 10$, and $Pe_h = 5$.**

(a) Reactant concentration profile. (b) Temperature profile.

with

$$x_{\min} = 1 - \frac{1}{Pe_m} \ln\left\{ \left(2 - \frac{Pe_m}{\varphi\,\phi^2}\right) Pe_m \ln\left[1 - \frac{2\varphi\,\phi^2}{Pe_m}\right] \right\}. \quad (79)$$

In the isothermal limit ($\varphi \to 0$), Eqs. 78 and 79 become:

$$x_{\min} \to 1 - \frac{\ln(2Pe_m)}{Pe_m} \quad (80)$$

and

$$c^{\min} \to -\frac{\phi^2}{Pe_m}\left(2 - \frac{\ln(2Pe_m)}{Pe_m} - \frac{1}{Pe_m}\right). \quad (81)$$

These results are in very good agreement with Eqs. 17 and 16 (which reproduce exact analytical solutions for isothermal conditions[3]).

*Concentration Annulment Inside the Particle (Regime IIIb).* Another important situation is the one in which the reactant concentration is depleted in a region inside the particle (Figure 4). The outer solution for the left region (Eq. 69) takes the zero concentration value at $\tilde{x} = -1 + Pe_m(1 - e^{-\varphi})/(\varphi\,\phi^2)$. For $x > \tilde{x}$, the solution should approach $c^m(x) = -1$ and the chemistry-free equations for temperature must be used (which predict uniform temperature profile). Finally, the diffusive-convective boundary layer (predicted from independent variable stretching in the previous section) allows the right boundary condition to be fulfilled. This structure can only exist if $\tilde{x}<1$ or

$$\frac{\phi^2}{Pe_m} > \frac{1 - e^{-\varphi}}{2\varphi}. \quad (82)$$

Because the left region solution Eqs. 68 and 69 predicts $c_0^l = -T_0^l$, profile continuity between the two branches of the solution will require $T_0^m = 1$. Matching of the boundary layer at $x = 1$ with the middle region implies: $a_1 = -a_2 = -1$. A smooth composite solution uniformly valid requires a more complex mathematical structure. Nevertheless, these three independent branches should be good estimates for the profiles in each region. We shall use these results to estimate the effectiveness factor in this regime.

In the isothermal limit of this strong convective regime, asymptotic expressions for the concentration annulment points are available[3]: $x' = -1 + Pe_m/\phi^2$ (left side) and $x^* = 1 - \ln(Pe_m^2/\phi^2)/Pe_m$ (right side). The first result is in agreement with the isothermal limit of $\tilde{x}$ (for $\varphi \to 0$). A perturbation analysis of the exact nonlinear equation from which $x^*$ is calculated, suggests rescaling of $(1 - x^*)$ by $\varepsilon = 1/Pe_m$ and is therefore consistent with the thickness of the boundary layer predicted in the previous section.

*Transition Between Regimes II and IIIb.* Comparing the solution structure described earlier (for Regime IIIb) with the one built for diffusional regime (Regime II), it is possible to obtain simple order of magnitude relations concerning the transition between these two particular limits. Although both situations refer to high Thiele modulus, solutions of Eqs. 40 and 41 were found for $Pe_m$, $Pe_h \sim 1$, whereas the results obtained for Regime IIIb only have meaning when convection is high. Nevertheless, when the thicknesses of the regions near $x = -1$ become comparable ($x' \sim \tilde{x}$):

$$Pe_m \sim \sqrt{2}\,\phi\,\frac{\varphi}{b(1 - e^{-\varphi})} \quad (83)$$

with $b$ given by Eq. 61.

In the isothermal limit, Eq. 83 yields $Pe_m \sim \sqrt{2}\,\phi$. This means that, at high Thiele modulus, the effect of convection is felt only for $Pe_m > \phi$. The corrective factor in Eq. 83 applies when an exothermic reaction is occurring and increases the mass Peclet number needed for the effect of convection to be observed, when $Le > b/(\gamma\,\beta)$.

At the right surface, we require the position $x^*$ in the diffusional regime to be of the same order of the diffusive-convective boundary layer thickness, when convection is strong $(1/Pe_m)$. This implies $Pe_m \sim b\,\phi/\sqrt{2}$ or

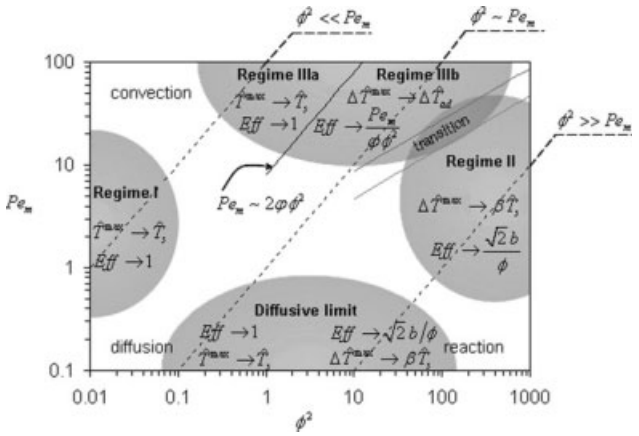


**Figure 9. Regime diagram for an exothermic zero-order reaction in permeable catalyst slab.**

Shown are the leading-order estimates for the effectiveness factor and maximum temperature in each of the studied regimes, for $Le \sim 1$. Approximate boundaries between strong convective-reactive regimes are also presented.

$Pe_m \sim \phi/\sqrt{2}$ (isothermal reaction). A transition region around these curves can be represented for the isothermal case (see Figure 1) and for the exothermic case (Figure 9).

### *Maximum temperature estimate*

When mass/heat transfer occurs solely by diffusion/conduction, it is possible to establish a simple relationship between concentration and temperature profiles, from which an a priori estimate for the maximum temperature can be obtained.[25,26] Such result provides a useful measure for internal nonisothermal effects, and an indication on whether the temperature exceeds some critical value for operation or not.

For the regimes outlined earlier, it is possible to obtain estimates for the maximum temperature attained in the particle, when convection is also present (Table 1). At low Thiele modulus (Regimes I and IIIa), the temperature inside the particle is close to the surface value (Eqs. 87 and 91). For materials with high conductivity or when no convection exists ($Pe_h \to 0$), $\hat{T}^{max} \to \hat{T}_s$. It can be shown that according to Eq. 87: $\hat{T}^{max}/\hat{T}_s \to 1 + \beta\,\phi^2/2$ (for $\phi^2 << 1$). On the other hand, for poorly conductive catalysts $Pe_h \to \infty$, $\hat{T}^{max}/\hat{T}_s \to 1 + 2\,\beta\,\phi^2/Pe_h$.

Under "diffusional regime" conditions, the correction brought by convection to the diffusive leading-order result $\left(\hat{T}^{max} = \hat{T}_s(1+\beta)\right)$ is of order $\sqrt{\varepsilon} = \sqrt{Pe_m}/\phi$. For $Le = 1$, the maximum temperature change (Eq. 89) reduces to the characteristic diffusive value, which equals the adiabatic temperature rise.

In Regime IIIb, where convection is strong and the solution includes a region where annulment occurs, the maximum temperature is obtained at the same position where concentration reaches annulment (no increase is expected in the middle solution, which is a plateau, or in the boundary layer). It may be shown (Eq. 94) that the maximum temperature change is equal to the adiabatic temperature rise after complete reaction in a catalyst slab with initial uniform surface-like reactant concentration $\left(T^{max} \sim -c^{min} \sim 1\right)$: $\hat{T}^{max}/\hat{T}_s \sim 1 + \beta\,Pe_m/Pe_h$. This was also obtained in the perturbation analysis for first-order reactions in the convective regime.[15] The leading-order estimates for maximum temperature, in each regime, are indicated in Figure 9.

### *Effectiveness factor approximation*

The performance of the catalyst particle in the regimes described may be quantified by the effectiveness factor, defined by Eq. 7. In general, the calculation is rather straightforward, especially in the regimes with uniformly valid solutions. So, differentiation of Eqs. 13, 41, and 76 yields direct estimates for the effectiveness factor in Regimes I, II, and IIIa, as shown in Table 1.

In the "chemical regime," the effectiveness factor is close to unity. Taking the limit of Eq. 86, when $Pe_h \to 0$ (when there is no convection or when the catalyst is highly conductive), gives $\text{Eff} \to 1 + \gamma\,\beta\,\phi^2/3$

This result is also obtained by perturbation analysis for a zero-order reaction, with no convection, in the low Thiele modulus regime. For strong convection ($Pe_h \to \infty$) or under isothermal conditions ($\beta \to 0$), the leading-order estimate is again Eff $\to 1$. The results for Regime IIIa (Eq. 90), where convection is strong, agree qualitatively with this result.

In the "diffusional regime," the leading-order estimate for the effectiveness factor (from Eq. 88) is

$$\text{Eff} = \frac{\sqrt{2}\,b}{\phi}. \tag{84}$$

We expect this result to agree with the effectiveness factor calculated for the explosive branch[22] of the diffusion-reaction problem. This is the case if $b^2 \sim \left(e^{\gamma\beta} - 1\right)/(\gamma\,\beta)$ agrees with Eq. 61. The agreement is indeed very good, especially for $\gamma\,\beta < 2$. In the isothermal diffusive limit, Eq. 88 retrieves the well-known result, Eff $= \sqrt{2}/\phi$.

For Regime IIIb, an approximate result was obtained by considering the solution structure previously described. If we

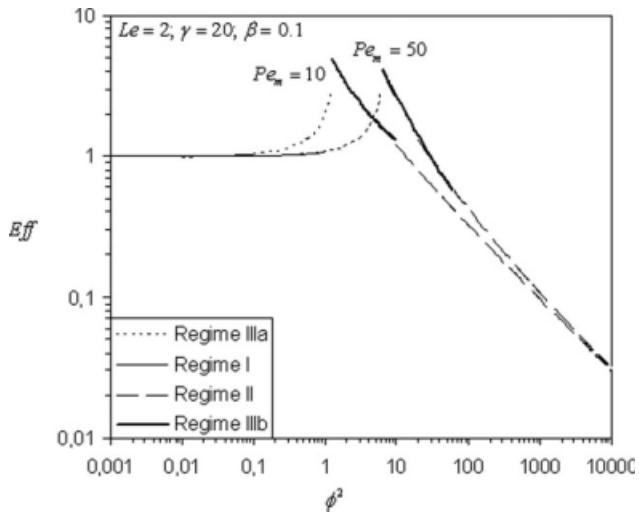


**Figure 10. Effectiveness factor plot in the four regimes studied (Eqs. 86, 88, 90, and 93).**

**Table 1. Effectiveness Factor and Maximum Temperature Approximations**

| | |
|---|---|
| Regime I<br>$\frac{\phi^2}{Pe_m} << 1, \frac{1}{Pe_m}, \frac{1}{Pe_h}$ | $\text{Eff} = 1 + \varphi \frac{\phi^2}{Pe_m}\left[\frac{e^{2Pe_h}+1}{e^{2Pe_h}-1} - \frac{1}{Pe_h}\right] + O\left(\frac{\phi^4}{Pe_m^3}\right)$ (86) |
| | $\frac{\hat{T}^{max}}{\hat{T}_s} = 1 + \beta \frac{\phi^2}{Pe_h^2}\left\{\frac{\ln[2\,e^{2Pe_h}]}{e^{2Pe_h}-1} + \ln\left[\frac{e^{2Pe_h}-1}{2Pe_h}\right] - 1\right\} + O\left(\frac{\phi^4}{Pe_m^2}\right)$ (87) |
| Regime II<br>$\frac{\phi^2}{Pe_m} >> 1, \frac{1}{Pe_m}, \frac{1}{Pe_h}$ | $\text{Eff} = \frac{\sqrt{2}\,b}{\phi} + \varphi \frac{Pe_m}{\phi^2}\left\lvert 1 - \frac{Pe_h}{Pe_m}\right\rvert \left(6\frac{Pe_m}{Pe_h} - \varphi\right)^{-1} + O\left(\frac{Pe_m}{\phi^4}\right)$ (88) |
| | $\frac{\hat{T}^{max}}{\hat{T}_s} = 1 + \beta\left(1 + \frac{\sqrt{2}Pe_m}{3\,b\,\phi}\left\lvert 1 - \frac{Pe_h}{Pe_m}\right\rvert\right) + O\left(\frac{Pe_m}{\phi^2}\right)$ (89) |
| Regime III<br>$\frac{\phi^2}{Pe_m} \sim 1$ and $\frac{1}{Pe_h}, \frac{1}{Pe_m} << 1$ | IIIa: For $\frac{2\,\varphi\,\phi^2}{Pe_m} < 1$, |
| | $\text{Eff} = \frac{Pe_m}{2\,\varphi\,\phi^2}\left(e^{-2Pe_m} - 1\right)\,\ln\left[1 - \frac{2\,\varphi\,\phi^2}{Pe_m}\right] - \frac{1}{Pe_m}\left[1 - \frac{2\,\varphi\,\phi^2}{Pe_m}\right]^{-1} + O\left(\frac{1}{\phi^2 Pe_m}\right)$ (90) |
| | $\frac{\hat{T}^{max}}{\hat{T}_s} = 1 - \frac{\beta}{\gamma}\ln\left[1 - \frac{\varphi\,\phi^2}{Pe_m}(x_{max}+1)\right] + \frac{\beta}{\gamma}\ln\left[1 - \frac{2\varphi\,\phi^2}{Pe_m}\right] e^{-Pe_h(1-x_{max})}$ (91) |
| | with $x_{max} = 1 - \frac{1}{Pe_h}\ln\left\{\left(2 - \frac{Pe_m}{\varphi\,\phi^2}\right)Pe_h \ln\left[1 - \frac{2\varphi\,\phi^2}{Pe_m}\right]\right\}$ (92) |
| | IIIb: For $\frac{\phi^2}{Pe_m} > \frac{1-e^{-\varphi}}{2\varphi}$, |
| | $\text{Eff} = \frac{Pe_m}{2\phi^2} + \frac{3+e^{\varphi}}{4Pe_m} + \frac{\phi^2}{Pe_m}\frac{\varphi}{2Pe_m^2} + O\left(\frac{1}{Pe_m^3}\right)$ (93) |
| | $\frac{\hat{T}^{max}}{\hat{T}_s} \sim 1 + \beta\,\frac{Pe_m}{Pe_h} + O\left(\frac{\beta}{Pe_m}\right)$ (94) |

where: $b^2 = \sqrt{\pi}\exp(\gamma\,\beta)\,erf\sqrt{\gamma\,\beta}/\left(2\sqrt{\gamma\,\beta}\right)$ and $\varphi = \gamma\,\beta\,Pe_m/Pe_h$.

use a two-term expansion to describe the concentration profile in each region, Eq. 7 yields:

$$\text{Eff} \sim \frac{1}{2\phi^2}\left(\left.\frac{dc_0^r}{dx}\right|_{x=1} + \varepsilon\left.\frac{dc_1^r}{dx}\right|_{x=1} - \left.\frac{dc_0^l}{dx}\right|_{x=-1} - \varepsilon\left.\frac{dc_1^l}{dx}\right|_{x=-1}\right). \quad (85)$$

We note that $c_0^l(x)$ is given by Eq. 69 and $c_0^r(x)$ by Eq. 107 with $a_1 = -1$. To evaluate the remaining terms in Eq. 85, we calculate $c_1^l(x)$ from the $O(\varepsilon)$ subproblem and $dc_1^r/dx\big|_{x=1}$ is obtained integrating the $O(\varepsilon)$ mass balance over the boundary layer with thickness $\varepsilon \sim 1/Pe_m$. That is, for $\eta T_0^r << 1$:

$$\left.\frac{dc_1^r}{dx}\right|_{x=1} = \frac{1}{\varepsilon^2}\frac{\phi^2}{Pe_m}\int_{1-1/Pe_m}^{1}\exp\left[\varphi T_0^r\right]dx \sim \frac{1}{\varepsilon^2}\frac{\phi^2}{Pe_m}\frac{e^{\varphi}+1}{2}\left(\frac{1}{Pe_m}\right)$$

where the integral on the right-hand side of this equation is evaluated using the trapezoidal rule between the surface and the maximum temperature values. Substituting these results into Eq. 85, gives an estimate for the effectiveness factor in

Regime IIIb (Eq. 93). If we take the limit of Eq. 93 for $\varphi \to 0$ ($\beta \to 0$), we obtain

$$\text{Eff} \sim \frac{Pe_m}{2\phi^2} + \frac{1}{Pe_m}$$

This solution is in excellent agreement with the asymptotic limit for high $Pe_m$ (maximum error of 5% for $Pe_m \sim \phi^2 \sim 10$) presented by Rodrigues et al.[3] for the isothermal case. Also, for strong convection the maximum effectiveness factor is given by $\text{Eff} \sim Pe_m/(2\phi^2)$. This result also appeared in the analysis for first-order reaction by Cardoso and Rodrigues,[15] although they were able to find the full concentration and temperature profiles in this regime. In these cases and when mass and thermal diffusivities are comparable, the performance of the catalyst depends at $O(1)$ on the Thiele modulus and intraparticular mass Peclet number but not on any information regarding heat transfer or generation mechanisms ($\varphi$ or $Pe_h$). Note that, for strong convective regimes, the contribution of the profile near $x = -1$ for the effectiveness factor is negligible, because reactant concentration decay is slow at the slab's entrance. All these results are summarized in Table 1 and plotted in Figure 10.

## Conclusions

The analysis of simultaneous convection, diffusion, and reaction is presented for an exothermic zero-order reaction occurring in a catalyst slab. Scaling techniques yield simple order of magnitude estimates for the characteristic temperature change experienced. We identified the regions in which the system behaves as isothermal, diffusive, adiabatic, or "explosive" by a 3D regime diagram. In particular, we study the limits of chemical and diffusional regimes, in the presence of convection, and a strong convective regime, by conducting suitable perturbation analysis. For each regime, estimates of the effectiveness factor and maximum temperature are provided (Figure 9). They are consistent with the isothermal and diffusive limits, and agree with previous approximate analytical analysis.[15] When intraparticular convection is the dominating transport mechanism in a system with $Le \sim 1$, the performance of the catalyst depends (to a first approximation) on the mass Peclet number and Thiele modulus, but not on heat generation or transport. The maximum temperature was found to coincide with the adiabatic temperature change that one would observe after complete reaction, in a catalyst slab with initial uniform surface-like concentration and temperature.

## Notation

$a_1, a_2$ = integration constants in Eqs. 70 and 71
$b$ = parameter defined in Eq. 61
$c$ = dimensionless concentration of reactant
$c_n(x)$ = perturbation function of order $n$ for dimensionless concentration
$\hat{c}$ = concentration of reactant
$\hat{c}_s$ = concentration at the surface of the slab
$C_p$ = specific heat of the catalyst matrix filled with fluid
$d$ = parameter defined in Eq. 62
$D$ = effective reactant mass diffusivity
$E_{act}$ = reaction activation energy
Eff = effectiveness factor
$erf(z)$ = "error function," defined by $erf(z) = \frac{2}{\sqrt{\pi}} \int_0^z e^{-t^2}\, dt$
$f$ = parameter defined in Eq. 63
$(-\Delta H)$ = heat of the exothermic reaction
$k$ = intrinsic kinetic constant
$k_s$ = kinetic rate constant evaluated at the surface temperature of the catalyst
$L$ = semi-thickness of the slab
$Le$ = Lewis' number ($= \kappa/D$)
$Pe_h$ = intraparticular heat Peclet number ($= uL/\kappa$)
$Pe_m$ = intraparticular mass Peclet number ($= uL/D$)
$r(T)$ = dimensionless reaction term defined by Eq. 6
$R$ = ideal gas constant
$T$ = dimensionless temperature
$T_n(x)$ = perturbation function of order $n$ for dimensionless temperature
$\hat{T}$ = temperature
$\hat{T}_s$ = temperature at the surface of the slab
$\Delta\hat{T}$ = characteristic temperature change
$\Delta\hat{T}_{ad}$ = adiabatic temperature change, which is given by the product of the heat of reaction and surface concentration divided by the specific heat and by the mass density
$\Delta\hat{T}_{dif}$ = maximum temperature change observed in a diffusive-reactive system with concentration annulment
$u$ = superficial fluid velocity
$x$ = dimensionless transverse position within the slab
$\hat{x}$ = transverse position within the slab
$x'$ = position where concentration reaches annulment on the left side of the slab
$x^*$ = position where concentration reaches annulment on the right side of the slab
$\tilde{x}$ = point where outer solution in Eqs. 69 takes zero concentration value
$X$ = stretched coordinate in the region near $x = 1$ in Eq. 22
$X^*$ = stretched annulment position near $x = 1$
$X_n^*$ = coefficients in the expansion for $X*$
$Y$ = stretched coordinate in the region near $x = -1$
$Y'$ = stretched annulment position region near $x = -1$
$Y_n'$ = coefficients in the expansion for $Y'$

### Greek letters

$\beta$ = Prater's parameter $(= (-\Delta H) D\, \hat{c}_s/(\rho\, C_p\, \kappa\, \hat{T}_s))$
$\delta$ = thickness of the boundary layer
$\epsilon$ = small (perturbation) parameter
$\phi$ = Thiele modulus $(= L\sqrt{k_s/(\hat{c}_s D)})$
$(\phi^2)_{crit}$ = critical Thiele modulus value, above which concentration annulment occurs
$\gamma$ = Arrhenius parameter $(= E_{act}/(R\hat{T}_s))$
$\eta$ = characteristic temperature change normalized by surface temperature $(= \Delta\hat{T}/\hat{T}_s)$
$\varphi$ = nonisothermal parameter $(= \gamma\eta)$
$\kappa$ = fluid-filled catalyst effective thermal diffusivity $(= \lambda/\rho C_p)$
$\lambda$ = effective thermal conductivity of the fluid-filled catalyst
$\rho$ = density of the catalyst matrix filled with fluid

### Subscripts

max = maximum
min = minimum
$n$ = order of the perturbation function

### Superscripts

comp = composite
$l$ = left
$m$ = middle
max = maximum
min = minimum
$r$ = right


## Acknowledgements

Financial support from FCT - Fundação para a Ciência e a Tecnologia, PhD fellowship SFRH/BD/36833/2007 is acknowledged.

## Literature Cited


1. Wheeler A. Reaction rates and selectivity in catalyst pores. *Adv Catal*. 1951;3:249–327.
2. Nir A, Pismen LM. Simultaneous intraparticle forced convection, diffusion and reaction in a porous catalyst. *Chem Eng Sci*. 1977;32:35–41.
3. Rodrigues AE, Orfao JM, Zoulalian A. Intraparticle convection, diffusion and zero order reaction in porous catalysts. *Chem Eng Commun*. 1984;27:327–337.
4. Stephanopoulos G, Tsiveriotis K. Effect of intraparticle convection on nutrient transport in porous biological pellets. *Chem Eng Sci*. 1989;44:2031–2039.
5. Fassnacht D, Pörtner R. Experimental and theoretical considerations on oxygen supply for animal cell growth in fixed-bed reactors. *J Biotechnol*. 1999;72:169–184.
6. Goldstein AS, Juarez TM, Helmke CD, Gustin MC, Mikos AG. Effect of convection on osteoblastic cell growth and function in biodegradable polymer foam scaffolds. *Biomaterials*. 2001;22:1279–1288.
7. Young MW, Dean RC. Optimization of mammalian-cell bioreactors. *Bio-Technology*. 1987;5:835–837.
8. Martin Y, Vermette P. Bioreactors for tissue mass culture: Design, characterization, and recent advances. *Biomaterials*. 2005;26:7481–7503.
9. Coletti F, Macchietto S, Elvassore N. Mathematical modeling of three-dimensional cell cultures in perfusion bioreactors. *Indust Eng Chem Res*. 2006;45:8158–8169.
10. Chung CA, Chen CW, Chen CP, Tseng CS. Enhancement of cell growth in tissue-engineering constructs under direct perfusion: Modeling and simulation. *Biotechnol Bioeng*. 2007;97:1603–1616.
11. Allen JW, Bhatia SN. Formation of steady-state oxygen gradients in vitro: Application to liver zonation. *Biotechnol Bioeng*. 2003;82:253–262.
12. Prince CL, Bringi V, Shuler ML. Convective mass transfer in large porous biocatalysts: Plant organ cultures. *Biotechnol Progr*. 1991;7:195–199.
13. Quinta Ferreira RM. Contribuição para o Estudo de Reactores Catalíticos de leito fixo. Efeito da convecção em catalisadores de poros largos e casos de catalisadores bidispersos. Porto, University of Porto; 1988.
14. Lopes JCB, Dias MM, Mata VG, Rodrigues AE. Flow field and non-isothermal effects on diffusion, convection, and reaction in permeable catalysts. *Indust Eng Chem Res*. 1995;34:148–157.
15. Cardoso SSS, Rodrigues AE. Convection, diffusion and reaction in a nonisothermal, porous catalyst slab. *AIChE J*. 2007;53:1325–1336.
16. Cardoso SSS, Rodrigues AE. Diffusion and reaction in a porous catalyst slab: Perturbation solutions. *AIChE J*. 2006;52:3924–3932.
17. Lin CC, Segel LA. Mathematics applied to deterministic problems in the natural sciences. *SIAM*. 1988:185–224.
18. Rodrigues AE. *Scientific bases for the design of two-phase catalytic reactors*. In: Rodrigues AE, Calo JM, Sweed NH, editors. *Multiphase Chemical Reactors—Design Methods*, Vol. 2. Rockville, MD: NATO ASI Series E-52, 1981:65–133.
19. Bender CM, Orszag SA. *Advanced Mathematical Methods for Scientists and Engineers*. New York: Springer-Verlag, 1999.
20. Frank-Kamenetskii DA. *Diffusion and Heat Exchange in Chemical Kinetics*. Princeton: Princeton University Press, 1955.
21. Hlavacek V, Marek M. Modelling of Chemical Reactors .V. Heat and mass transfer within a porous catalyst particle—Some results of an analysis for a zeroth-order reaction. *Collect Czech Chem Commun*. 1967;32:4004–4017.
22. Aris R. *The Mathematical Theory of Diffusion and Reaction in Permeable Catalysts*. Vol 1. London: Oxford University Press, 1975.
23. *gPROMS*[computer program]. Version 3.0.3. London, 2007.
24. Marek M, Hlavacek V. Modelling of chemical reactors.VI. Heat and mass transfer in a porous catalyst particle; On the multiplicity of solutions for the case of an exothermic zeroth-order reaction. *Collect Czech Chem Commun*. 1968;33:506–517.
25. Damkohler G. The excess temperature in contact grains. *Zeitschrift Fur Physikalische Chemie-Leipzig*. 1943;193:16–28.
26. Prater CD. The temperature produced by heat of reaction in the interior of porous particles. *Chem Eng Sci*. 1958;8:284–286.


*Manuscript received Oct. 16, 2008, revision received Dec. 3, 2008, and final revision received Jan. 7, 2009.*